Journal of Molecular and Cellular Cardiology Plus 12 (2025) 100300

Contents lists available at ScienceDirect

Journal of Molecular and Cellular Cardiology Plus

journal homepage: www.journals.elsevier.com/journal-of-molecular-andcellular-cardiology-plus

Independent and synergistic roles of MEK-ERK1/2 and PKC pathways in regulating functional changes in vascular tissue following flow cessation

Spyridoula Kazantzi [a,b,*], Lars Edvinsson [c], Kristian Agmund Haanes [a,b,d]

[a] Sensory Biology Unit, Translational Research Centre, Copenhagen University Hospital – Rigshospitalet, Glostrup, Denmark
[b] Section of Cell Biology and Physiology, Department of Biology, University of Copenhagen, Denmark
[c] Division of Experimental Vascular Research, Department of Clinical Sciences, Lund University, Lund, Sweden
[d] Danish Headache Center, Department of Neurology, Copenhagen University Hospital – Rigshospitalet, Glostrup, Denmark

ARTICLE INFO

Keywords:
MEK-ERK1/2 pathway
PKC pathway
Ischemia
Flow cessation
Vasoconstriction
ET_B upregulation

ABSTRACT

Background: The MEK-ERK1/2 and PKC pathways play critical roles in regulating functional changes in tissues, but their interplay remains poorly understood. The vasculature provides an ideal model to study these pathways, particularly under conditions of flow cessation, which is highly relevant to ischemia and other cardiovascular diseases. This study examined the independent roles, additive effects, and time-dependent dynamics of MEK and PKC pathway inhibition in functional receptor upregulation.

Methods: Rat basilar arteries were cultured for 48 h with selective inhibitors targeting MEK (Trametinib), PKC (RO-317549) and their downstream ERK (Ulixertinib) and NF-kB (BMS 345541). Functional changes in ET_B receptor responses were assessed via wire myography following stimulation with Sarafotoxin 6c (S6c). Western blot analysis quantified ERK phosphorylation, and the effects of inhibitor timing and combination treatments were evaluated.

Results: MEK inhibition reduced ERK phosphorylation and ET_B receptor-mediated contractility, whereas PKC inhibition had no effect on ERK phosphorylation but significantly reduced ET_B receptor function. Combining MEK and PKC inhibitors produced an additive effect, resulting in greater suppression of functional changes compared to single treatments. At 6 h following flow cessation, PKC inhibition effectively suppressed ET_B receptor function, while MEK inhibition had minimal effects when introduced at this delayed time point.

Conclusions: The MEK and PKC pathways independently drive functional changes in vascular tissue, particularly following flow cessation. MEK inhibition is effective early, while PKC inhibition remains effective when applied later. The additive effects observed with combined MEK and PKC inhibition indicate parallel and functionally independent pathway activation during ET_B receptor upregulation.

1. Introduction

Ischemia resulting from flow cessation is a critical event that induces pathological changes in blood vessels, particularly in vascular smooth muscle cells, which are integral components of the vessel wall [1]. These changes involve receptor upregulation and functional alterations, impairing blood flow regulation [2]. While ischemia impacts all tissues, its consequences are particularly severe in the brain, where the regulation of cerebral blood flow is essential. In the context of ischemic stroke, the basilar artery (BA) is directly involved in the disease process and serves as a key structure for understanding these mechanisms, with broader implications for other vascular beds. Previous work by Edvinsson et al. demonstrated that protein kinase activation is associated with the early upregulation of endothelin B (ET_B) receptors, a process that can be mitigated by pathway-specific inhibition [3].

Flow cessation, whether due to large vessel occlusion, aneurysm

Abbreviations: AP-1, Activator Protein-1; BA, Basilar Artery; DCI, Delayed phase of global cerebral ischemia; DMEM, Dulbecco's Modified Eagles Medium; DMSO, Dimethyl Sulfoxide; ERK, Extracellular signal-regulated kinase; ET_B, Endothelin receptor type B; GAPDH, Glyceraldehyde 3-phosphate dehydrogenase; IKK, IκB Kinase; MAPK, Mitogen-activated protein kinase; MCA, Middle cerebral artery; MEK, Mitogen-activated protein kinase kinase; NF-κB, Nuclear factor kappa-light-chain-enhancer of activated B cells; OC, Organ Culture; PKC, Protein kinase C; S6c, Sarafotoxin 6c; VSMC, Vascular Smooth Muscle Cell.

* Corresponding author at: Sensory Biology Unit, Translational Research Centre, Copenhagen University Hospital – Rigshospitalet, Nordstjernevej 42, 2600 Glostrup, Denmark.

E-mail address: spyridoula.kazantzi@regionh.dk (S. Kazantzi).

https://doi.org/10.1016/j.jmccpl.2025.100300
Received 8 April 2025; Received in revised form 28 April 2025; Accepted 28 April 2025
Available online 30 April 2025

rupture, or other ischemic events, initiates pathological processes that can lead to worsening outcomes over time. In the brain, this is exemplified by delayed cerebral ischemia (DCI) following aneurysmal subarachnoid hemorrhage (aSAH) [4], where vessel narrowing, microthrombosis, and neuroinflammation contribute to the disease phenotype. A critical feature of these pathological processes is the upregulation of ET_B receptors, which normally reside on endothelial cells and mediate nitric oxide-dependent vasodilation [5–7]. During ischemia, however, ET_B receptors undergo a phenotypic shift, becoming upregulated on vascular smooth muscle cells, where they drive abnormal vasoconstriction. This shift, studied with the ET_B agonist Sarafotoxin (S6c) in vivo has been observed in coronary arteries [8,9], but the clinical and preclinical work has focused on stroke patients, animal models of focal ischemia, and flow cessation models, including organ culture studies [10–12].

Organ culture (OC), which involves incubating arteries without flow for 24–48 h, is a robust and well-established model for studying receptor upregulation and the resulting functional changes, isolating the effects of flow cessation, without the loss of O_2 and nutrients [13–15]. This approach enables the assessment of functional receptor responses, such as contractility, which represents the functional readout, which is more clinically relevant than changes in gene or protein expression alone. Additionally, the involvement of the protein kinase C (PKC) pathway in ET_B receptor upregulation post-organ culture in rat middle cerebral arteries (MCA) and BAs has been well documented [12–15]. The mitogen-activated protein kinase kinase (MEK)/extracellular signal-regulated kinases (ERK)1/2 and PKC pathways have been identified as key contributors to ET_B receptor upregulation under ischemic-like conditions in vivo [16,17]. MEK inhibition, for instance, reduces ET_B receptor-mediated vasoconstriction following flow cessation models, as demonstrated with Trametinib [17,18]. Similarly, PKC inhibition has been shown to suppress receptor upregulation and the associated functional changes in cerebral arteries [12–16].

Cancer therapies have opened new avenues for understanding vascular changes under flow cessation. Trametinib, a MEK inhibitor [19], and Ulixertinib, an ERK inhibitor [20], allow detailed exploration of the MEK-ERK1/2 pathway, a central signaling cascade implicated in both cancer progression and vascular changes. RO-317549, a PKC inhibitor [21], sheds light on PKC-driven phosphorylation processes, while BMS 345541, targeting Nuclear factor kappa-light-chain-enhancer of activated B cells (NF-κB) [22], enables the study of its downstream regulatory role in signaling pathways.

Despite all the above advances, the precise relationship between the MEK-ERK1/2 and PKC pathways remains incompletely understood, particularly in terms of their interplay, timing, and potential synergistic effects. Both pathways regulate receptor changes, but understanding their dynamics following flow cessation is essential for identifying effective interventions. The present study investigates the dynamic interplay between the MEK-ERK1/2 and PKC pathways in receptor changes following flow cessation. By combining pharmacological inhibition, functional assays, and timing analyses, this work provides insights into pathway independence, synergistic effects, and the broader significance of these pathways in vascular pathologies. Furthermore, the inclusion of downstream targets such as ERK and NF-κB allows for a more comprehensive analysis of these signaling cascades, highlighting their interconnected roles, and offering opportunities for refined therapeutic approaches in vascular pathologies.

2. Methods

2.1. Experimental design

In this experimental setup, rat BAs were cultured in serum-free Dulbecco's Modified Eagle's Medium (DMEM) for 48 h, in atmospheric air (~21 % O2) and supplemented with 5 % CO_2. A range of pathway-specific inhibitors was applied either individually or in combination. Vascular contractility was assessed using wire myography to measure the response to S6c, and Western blot analysis was performed to confirm protein levels under different experimental conditions. Additionally, immunofluorescence was used to confirm the upregulation of ET_B receptors in the experimental setup.

2.2. Experimental animals

109 Male Sprague-Dawley rats (270–330 g) were purchased from Taconic, Denmark. The animals were housed in Euro standard Type VI cages with 123-lid covers in groups of five. They were maintained on a 12-h light/dark cycle, at a temperature of 22 °C (± 2 °C) and humidity of 55 % (± 10 %) in the Translational Research Centre, Rigshospitalet. Food and water were provided ad libitum, with the diet consisting of standard chow and nuts. All animals were acclimatized for one week before euthanasia in accordance with the guidelines of the European Communities Council (86/609/ECC). The procedure was approved by the Danish Animal Experimentation Inspectorate, and reported following ARRIVE 2.0 guidelines. The rats were sedated with a mixture of 70 % CO_2 and 30 % O_2, followed by euthanasia via decapitation.

2.3. Organ culture

Rat brains were excised immediately and placed in an ice-cold oxygenated sodium Krebs solution (Na^+ Krebs) composed of: 119 mM NaCl, 15 mM $NaHCO_3$, 4.6 mM KCl, 1.2 mM NaH_2PO_4, 1.2 mM $MgCl_2$, 1.5 mM $CaCl_2$, with 5.5 mM glucose. Basilar arteries were dissected from the brain in a Petri dish with ice-cold oxygenated Na^+ Krebs buffer under a microscope and cut into 1.5–2 mm long cylindrical segments. Then, the isolated basilar arterial segments (with one myograph wire inside) were cultured for 48 h at 37° C in humidified incubator containing atmospheric air (~21 % O_2) supplemented with 5 % CO_2, in 2 mL of Dulbecco's Modified Eagle's medium (DMEM) (Gibco #31966, DK) containing an antibiotic and antifungal mixture of penicillin and streptomycin. Specific inhibitors were used and were added at time 0 or in some cases, the media were changed after 6 h of incubation with pure DMEM. The inhibitors used were: Trametinib GSK 1120212 (MEK inhibitor, 10^{-10} M – 10^{-6} M, Selleck Chemicals, Houston, TX, USA), RO-317549 (PKC inhibitor, 10^{-8}–10^{-5} M, Merck Life Science A/S, DK), Ulixertinib BVD-523 (ERK inhibitor, 10^{-9}–10^{-5} M, Selleck Chemicals, Houston, TX, USA), Ravoxertinib GDC-0994 (ERK inhibitor, 10^{-6} M, Selleck Chemicals, Houston, TX, USA), Temuterkib LY3214996 (ERK inhibitor, 10^{-6} M, Selleck Chemicals, Houston, TX, USA), SP 100030 (dual inhibitor of NF-κB and Activator Protein (AP-1), 10^{-6} M, TOCRIS, UK), IMD 0354 (IKKbeta inhibitor ab144823, 10^{-6} M, abcam, UK), BMS 345541 (NF-κB inhibitor, IKK-2 and IKK-1 inhibitor, ab144822, 10^{-6}–10^{-5} M, abcam, UK), as well as combination of some of them. The incubated segments were subsequently either used for Western blot and immunohistochemistry or mounted in the myograph.

2.4. Myograph

296 Artery segments were mounted on a pair of 40 μm-diameter stainless steel wires on a Mulvany-Halpern wire myograph (Danish Myograph Technology A/S, Denmark) and were heated to 37 °C, a temperature which was maintained during the experiments. The myographs were connected to a PowerLab Unit and responses were sampled in LabChart™ (ADInstruments, UK). To obtain optimal conditions for active tension development, BA segments were stretched to an optimal pretension (2.3 mN) in a three-step process as previously found optimal [23], after 20 min of equilibration. The segments were allowed to stabilize for 20–30 min and kept at this standard tension during the entire period in the myograph. To ensure a stable pH 7.40, all myograph baths were continuously bubbled with 5 % CO_2 in 95 % O_2.

The vascular smooth muscle cell contractile function was confirmed by challenging the segments two times with a temperature-controlled

60 mM K^+ – Krebs solution (+37 °C) of the following composition: 59.5 mM NaCl, 15 mM $NaHCO_3$, 60 mM KCl, 1.2 mM NaH_2PO_4, 1.2 mM $MgCl_2$, 1.5 mM $CaCl_2$, with 5.5 mM glucose. Concentration-response curves were obtained by the cumulative application Sarafotoxin 6c (S6c) (Bachem, Switzerland), a specific ligand for the ET_B receptor in the concentration range of 10^{-13} to 10^{-7} M. All contractile responses are expressed as percentage of the maximal contraction induced by the K^+ response.

2.5. Western blot

Western immunoblotting was performed for assessment of the protein expression. Fresh and incubated basilar arterial segments (24) were immediately added to a RIPA lysis buffer (Apoteket, Region H, Denmark) and Laemmli SDS loading sample buffer (4× Laemmli Sample Buffer, Bio-Rad Laboratories. Cat. #1610747) heated to 95° C, for protein sample preparation. The samples were frozen and subsequently stored at -20° C for use the next day, or -80° C for longer term storage. The second day, the samples were sonicated and stored at -20 °C or -80 °C. For Western blotting, dithiothreitol reducing agent (DDT, Bio-Rad, Cat. #1610610) was added to the samples (5 %) and they were heated at 70 °C for 10 min 10 μL of the samples and 10 μL of SDS marker (Precision Plus Protein Kaleidoscope Prestained Protein Standards, Bio-Rad, Cat. #1610375) were loaded on the gel (Mini-PROTEAN TGX Precast Gels 4–20 % from Bio-Rad. Cat. #: 456–1093). Samples were run in gels in parallel at the electrophoresis chamber with the following settings: 200 V, 100mAMP/gel for >1 h. Proteins were transferred from the mini-gels in a 0.2 μm PVDF membrane (Trans-Blot Turbo Mini Transfer Pack, Cat. #: 1704156, Bio-Rad) using the Trans-Blot Turbo cassette.

The membranes were then transferred to a rocking table in room temperature with Blocking Buffer (EveryBlot Blocking Buffer, Cat. #: 12010020, Bio-Rad) for 10 min and then, the membranes were incubated with primary antibody dilutions overnight in 4 °C (1:1000 Mouse Anti-p44 / 42 MAP Kinase Monoclonal Antibody, Unconjugated, Clone L34F12 [Cell Signaling Technology Cat# 4696, lot: 29, RRID: AB_390780], 1:1000 Phospho-p44/42 MAPK (Erk1/2) (Thr202/Tyr204) (D13.14.4E) XP® Rabbit mAb [Cell Signaling Technology Cat# 4370, Lot: 28, RRID:AB_2315112), 1:1000 NF-κB p65 (L8F6) Mouse mAb [Cell Signaling Technology Cat# 6956, Lot:10, RRID:AB_10828935], 1:1000 Phospho-NF-κB p65 (Ser536) (93H1) Rabbit mAb [Cell Signaling Technology Cat# 3033,Lot: 19, RRID:AB_331284], GAPDH (D16H11) XP Rabbit mAb, [Cell Signaling Technology Cat# 5174, Lot: 8, RRID:AB_10622025], 1:1000 Actin, Smooth Muscle (1A4) Mouse Monoclonal Antibody [Cell Marque Cat# 202 M-94, Lot:0000243213, RRID:AB_1157937], 1:1000 alpha smooth muscle Actin antibody (EPR5368) [Abcam Cat# ab124964, Lot:GR303485–26, RRID:AB_11129103]). The following day the membranes were places on the rocking table for 10 min in room temperature and then washed 2 × 5 min with TBS – T buffer (10xTris Buffered Saline, Cat. #1706435, Bio-Rad, diluted in milliQ water with Tween20). The membranes were then transferred to secondary antibody dilution 1:3000 (Goat Anti-Rabbit IgG (H + L)-HRP Conjugate, [Bio-Rad Cat# 170–6515, RRID: AB_11125142], Goat Anti-Mouse IgG (*HL*)-HRP Conjugate, [(Bio-Rad Cat# 170–6516, RRID:AB_11125547]) for 1 h at room temperature. Then washed 5 × 3 minutes with TBS-T buffer, and 1 × 5 min with Distilled water. Bands were imaged using ECL (Clarity Western ECL Substrate: Clarity Western Peroxide Reagent and Clarity Western Luminol/Enhancer Reagent, Cat. #1705060, Bio-Rad) and imaged with Luminescent Image Analyzer, LAS-4000, Fujifilm, Tokyo, Japan). Due to the small size of the vessel segments, protein concentration could not be measured separately; therefore, normalization to the housekeeping protein GAPDH was applied to account for loading variability, in accordance with standard practice. The stability of GAPDH was confirmed by quantifying GAPDH to alpha-smooth muscle actin. Protein expression was quantified using ImageJ.

2.6. Immunohistochemistry and quantification

Fresh or 48 h incubated BA segments (1.5–2 mm) were fixed with 4 % paraformaldehyde solution for 15 min. The arteries were cryoprotected by incubation in 10 % sucrose (Merck, Germany) in Sorensen's phosphate buffer (0.1 M NaH_2PO_4 and 0.1 M Na_2HPO_4) for 24–48 h (+4 °C), followed by 25 % sucrose in Sorensen's phosphate buffer for minimum 24 h (+4 °C). The arteries were covered with Tissue-Tek O.C.T. (Gibco) in cryomold squares, frozen in dry ice and kept at -80 °C overnight. The next day the blocks were sectioned at a thickness of 10 μm on a cryostat (Leica CM3050 S, Leica Microsystems, Germany) and mounted on SuperFrost slides (Hounisen, Germany).

The arterial sections were thawed at room temperature and then rehydrated and washed with 0.05 % Tween20 diluted in PBS (PBS-T, Sigma) for 3 × 5 min. The sections were then permeabilized and blocked with blocking buffer (Triton X-100 (0.3 %), Bovine serum albumin (3 %) and glycine (0.3 M) in PBS) for 20 min and incubated for 5 min in Ab diluent (Triton X-100 (0.1 %) and BSA (1 %) in PBS). Incubation with 1:500 primary anti-endothelin B receptor / ET-B antibody (Rb polyclonal ET_B receptor antibody, ab117529, RRID:AB_10902070, Abcam) overnight in moisturized chambers. The following day, after the arteries were washed with the Ab diluent 3 × 5 min, the secondary antibody (1:500, Goat anti-Rabbit polyclonal IgG (H + L), Alexa Fluor 568, ab175471, RRID:AB_2576207, Abcam) added and incubated for 1 h at room temperature, in the dark to minimize loss of fluorescence. Excess secondary antibody was then washed with 0.05 % Tween20 diluted in PBS for 3 × 5 min. Nuclei were stained with antifading medium (Vectashield, Vector Laboratories, Burlingame CA, USA) containing 4′,6-diamidino-2-phenylindole (DAPI). Immunoreactivity was visualized and photographed with a Nikon microscope (Nikon Ti2-E).

Quantification of immunoreactivity was performed using ImageJ software (NIH). The acquired TIFF images were imported into ImageJ, and regions of interest were manually drawn around each artery, while carefully excluding any nonspecific surrounding tissue or arterial branches. Mean fluorescence intensity and the area of each selected region were measured. The immunofluorescence intensity (Arbitrary Units, A.U.) was normalized by dividing the mean intensity by the corresponding area.

2.7. Data and statistical analysis

Data were analyzed using GraphPad Prism software (GraphPad Software Inc., USA). The $E_{max(S6c)}$ values refer to maximum contraction calculated as a percentage of the contractile capacity of 60 mM K^+ and the pEC_{50} values refer to the negative logarithm of the molar concentration that produces half-maximum contraction. Data are expressed as mean values ± SEM, with *n* indicating the number of arterial segments from the brains of different rats. Statistical analyses, including *t*-test, one way and two-way ANOVA, were performed, with $p < 0.05$ considered significant. Post hoc tests were applied following ANOVA when the data were normally distributed when the variance was homogeneous. For statistics Student's *t*-test with/without a multiple correction (Holm-Sidak), repeated measures two-way ANOVA with Sidak's post-test, or one-way ANOVA with Dunnet's post-test was used. The statistical approach is specified in the legends testing used is indicated in each graph. Basilar segments showing contraction of <1 mN in response to 60 mM K^+ were considered non-viable and excluded from the analysis.

3. Results

3.1. Upregulation of ET_B in organ culture

We initially aimed to reconfirm the upregulation of the ET_B receptors in our experimental setup. Rat BAs, either freshly isolated or after a 48-h incubation in OC, were used to identify the differences at the ET_B receptor immunoreactivity (Fig. 1a). For the incubated BAs, the ET_B

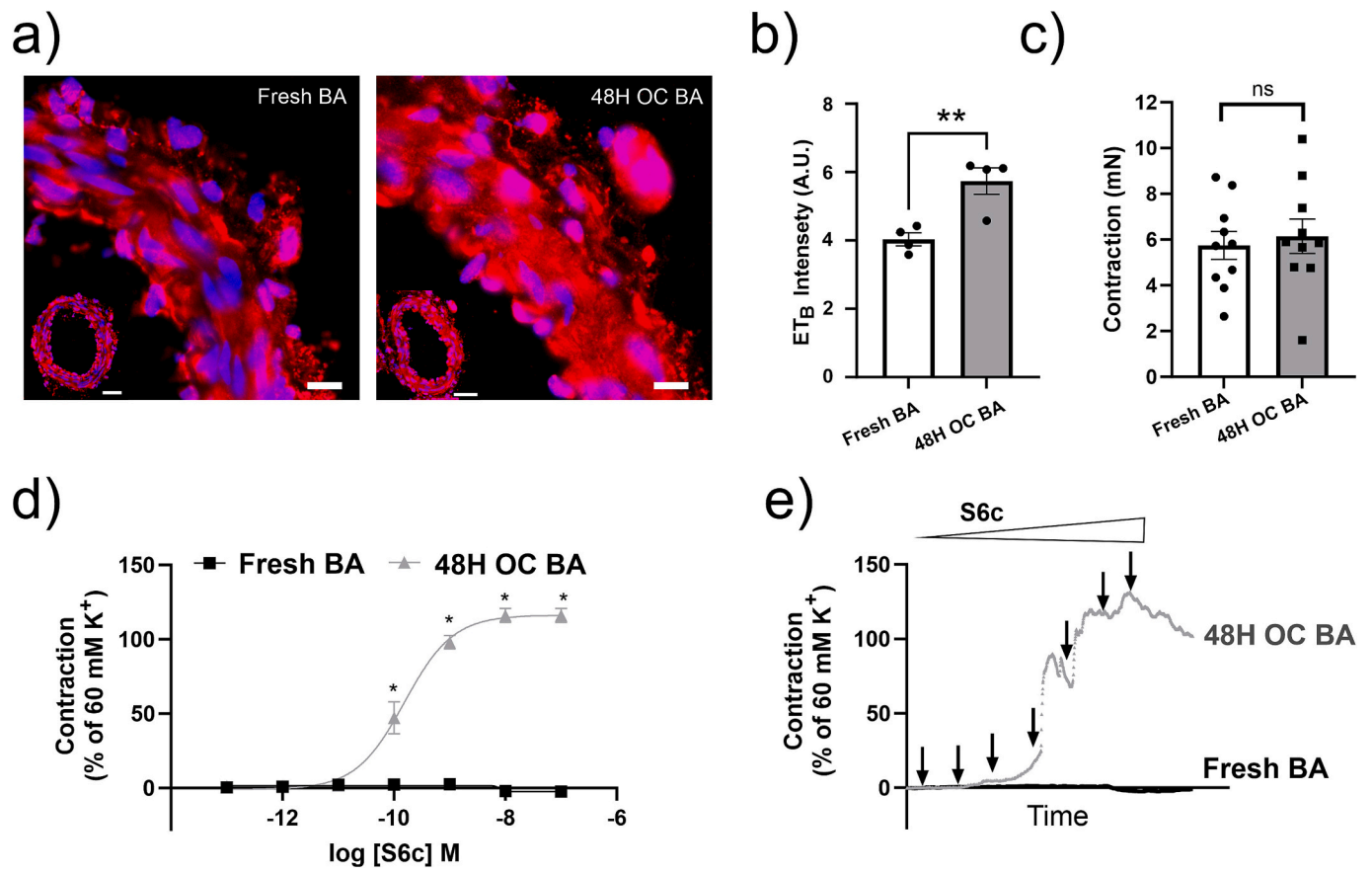

Fig. 1. Comparison of fresh BAs and BAs after 48 h of incubation in organ culture regarding ET_B receptors: (a) Immunofluorescence of ET_B receptors of the smooth muscle cell layer in fresh rat BAs and BAs after organ culture (48H) (b) Quantification of ET_B immunofluorescence, compared with Student's t-test (c) Contraction (mN) to 60 mM K^+, compared with Student's t-test (d) Log concentration-response curves in response to S6c, and values compared by repeated measures two-way ANOVA, with Sidak's post-test (e) Representative sample traces from LabChart. Effects of S6c Data show the contractile responses in rat BAs to cumulative contractions of sarafotoxin (S6c). Arrows indicate the times at which different concentrations were applied (Biological replicate; $n = 5–9$). * = $p < 0.05$.

expression (Fig. 1b) was more pronounced (5.7 ± 0.4 A.U) compared to the freshly isolated arteries (4.0 ± 0.2 A.U, $p = 0.008$). Moreover, myographic analyses were used in order to observe if this ET_B upregulation is connected to altered contractile responses. When stimulated with a depolarizing stimulus (60 mM K^+), both the fresh BAs (5.75 ± 0.6 mN) and the incubated BAs (6.15 ± 0.8 mN) showed similar contractile responses (Fig. 1c). However, we observed that when stimulated with sarafotoxin (S6c), an ET_B receptor agonist, the fresh BAs did not respond, whereas a strong contraction was observed in the incubated BAs ($E_{max(S6c)}$ = 116.1 ± 4.8 %) (Fig. 1d). S6c caused a sustained, concentration-dependent contraction in the incubated BAs, as shown in the representative sample traces (Fig. 1e). This finding supports the upregulation of the ET_B receptors in rat BAs following a 48-h OC.

3.2. *Inhibition of MEK and PKC influence the phosphorylation of ERK and NF-κB*

Both the MEK inhibitor Trametinib and the PKC inhibitor RO-317549 (RO-31) when present in the OC media, can prevent the occurrence of contractility in response to S6c [16–18]. However, the connection between these two pathways is not well studied. To investigate the acute phase of the upregulation, a 6-h timepoint was selected based on previous studies demonstrating that phosphorylation of ERK1/2 and activation of NF-κB pathways are detectable within the early hours of organ culture [24,25], and we further confirmed that ERK and NF-κB phosphorylation was observed at 1, 3, and 6 h (Supplementary Fig. 1a). The 6-h timepoint is also clinically relevant, corresponding to a phase where current pharmacological treatments for embolic stroke is not applicable [26,27].

Therefore, Western blot analysis was performed on arterial segments after incubation in the OC for 6 h. BAs were incubated with DMEM (control), 10^{-6} M of Trametinib or 10^{-5} M of RO-31. The incubation of the BAs with vehicle (control BAs) resulted in activation and phosphorylation of ERK (Fig. 2a). The presence of the MEK inhibitor, Trametinib, did not affect the total amount of the ERK ($p = 0.9$), however it diminished the ERK phosphorylation ($p = 0.02$), (Fig. 2b). In contrast, the PKC inhibitor, RO-31, did not affect the phosphorylation of ERK compared with the control (p = 0.9). Therefore, ERK phosphorylation is only prevented by a MEK inhibitor, whereas PKC inhibition does not affect pERK.

To ensure that the transcription factor activation can be affected by the PKC inhibitor, we decided to test one known transcription factor activated by PKC phosphorylation; NF-κB. At the control BAs, activation, and phosphorylation of NF-κB was observed (Fig. 2c). The total amount of NF-κB was not affected by the presence of RO-31 ($p = 0.8$), however the pNF-κB was reduced compared to control ($p = 0.03$). In contrast, Trametinib compared to control, did not affect either the total ($p = 0.7$) or the pNF-κB ($p = 0.16$) (Fig. 2d). We also confirmed that GAPDH was unaffected by the 6-h of OC compared to alpha-smooth muscle actin, highly abundant protein in VSMCs (Supplementary fig. 1b).

3.3. *Effect of the MEK and PKC inhibition to the ET_B upregulation*

To further evaluate the possible interplay between the MEK and PKC pathways, we set out to generate a full concentration response curve for Trametinib and RO-31 in the OC model, to determine their minimum

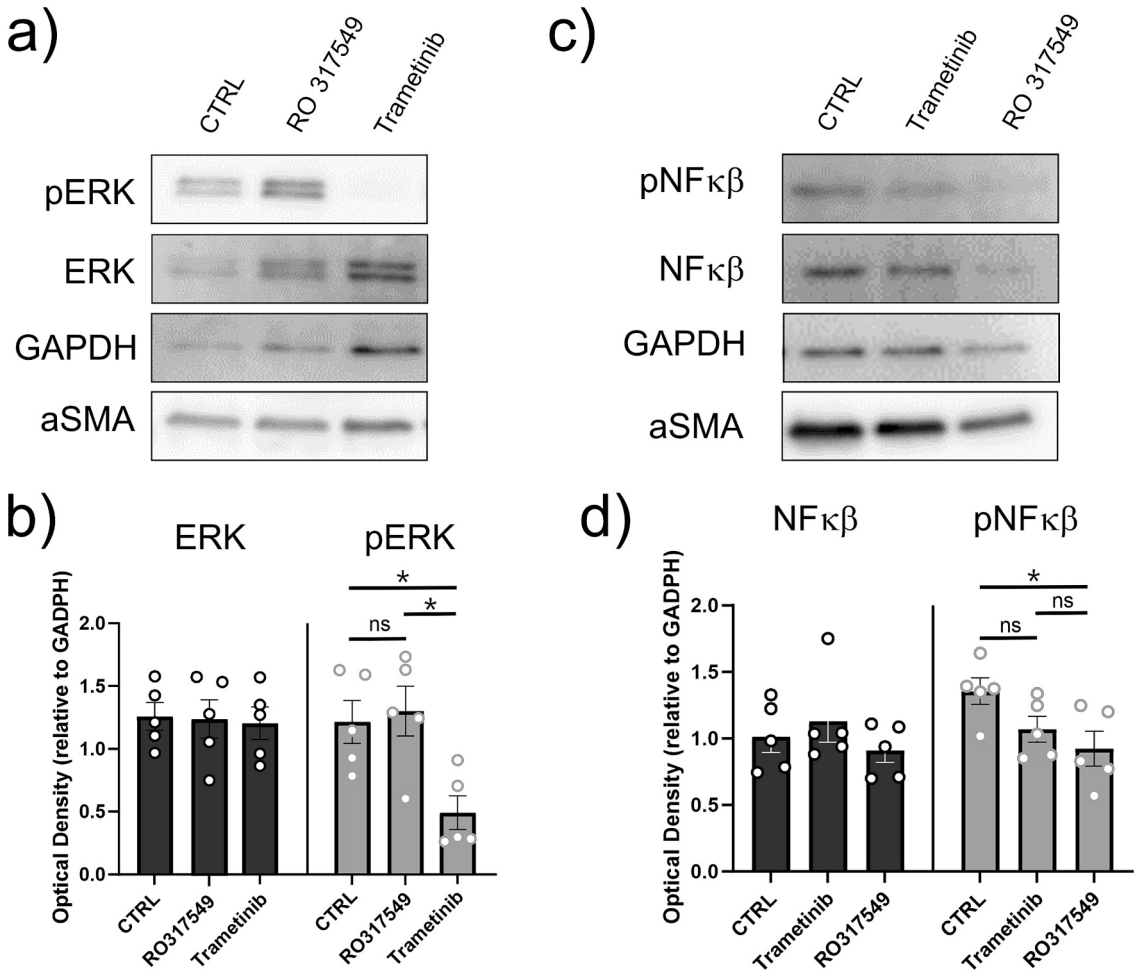

Fig. 2. Effects of the MEK inhibitor, Trametinib, and PKC inhibitor, RO-317549, on ERK and NF-κB phosphorylation. BAs were incubated in OC for 6 h. (a) Western blot analysis of total ERK and p-ERK, (b) Quantitative data of ERK, (c) Western blot of total NF-κB and pNF-κB (d) Quantitative data of NF-κB Data are shown as mean ± SEM (Biological replicate; $n = 5$) and protein expression was compared by one-way ANOVA, with Dunnett's post-test. * = $p < 0.05$. Please note that the order of the inhibitor is not the same across the figures, due to the original experimental setup.

effective concentration. To create a concentration response evaluation of Trametinib (10^{-10}–10^{-6} M), we incubated the BAs, and evaluated the contractility after 48 h, with S6c. There was no significant effect of MEK inhibition on the general contractility, assessed using 60 mM K^+ (supplementary table 1). For S6c, a strong contraction was observed in the BAs incubated in the presence of vehicle (DMSO) ($E_{max(S6c)}$ = 94.7 ± 10.6 %). The two lowest concentrations of Trametinib did not affect the S6c contraction (10^{-10} M, $E_{max(S6c)}$ = 108.8 ± 2 % and 10^{-9} M, $E_{max(S6c)}$ = 96.9 ± 5.5 %), whereas the first significant inhibitory effect was observed for the BAs incubated with 10^{-8} M of Trametinib ($E_{max(S6c)}$ = 72.8 ± 5.4 %, $p = 0.006$). The inhibitory effect was further enhanced at 10^{-7} M of Trametinib ($E_{max(S6c)}$ = 7.1 ± 2.1 %), while no further inhibition was possible with 10^{-6} M of Trametinib ($E_{max(S6c)}$ = 7 ± 3 %) (Fig. 3a). Hence, the concentration of 10^{-8} M is the minimum single effective concentration of Trametinib (Fig. 3b).

At the following experiment, a concentration response evaluation of RO-31 (10^{-8}–10^{-5} M) was performed. The general contractility induced by 60 mM K^+ was not affected by the PKC inhibitor (supplementary table 1). The data showed that there was a relationship between the increasing concentration of the inhibitor RO-31 in the 48-h OC and the disappearance of the S6c-mediated contraction in the myograph (Fig. 3c). In the BAs incubated in the presence of vehicle, a strong contraction was observed ($E_{max(S6c)}$ = 111.4 ± 4.7 %). No significant inhibitory effect was observed at the BAs incubated with 10^{-8} M of RO-31 ($E_{max(S6c)}$ = 108.4 ± 12.2 %, $p = 0.76$) or 10^{-7} M RO-31 ($E_{max(S6c)}$ = 110.6 ± 10 %, $p = 0.9$). However, for the BAs incubated with 10^{-6} M of RO-31 ($E_{max(S6c)}$ = 106.1 ± 5 %, $p = 0.48$), a significant reduction in contractility at 10^{-10} M S6c (Mean = 2.34 ± 0.85 %, $p < 0.001$), and 10^{-9} M S6c (Mean = 65.7 ± 11 %, $p < 0.001$) was observed. The shift in the contractility was also evident when comparing the $logEC_{50}$–9.141 (95 % CI: −9.27 to −9.03) of the BAs incubated with 10^{-6} M RO-31, with the concentration response curve to S6c of the BAs incubated in the presence of vehicle ($logEC_{50}$–9.813 (95 % CI: −9.96 to −9.63). The 10^{-5} M of RO-31 in the OC, abolished the contractile effect to S6c completely ($E_{max(S6c)}$ = 0.46 ± 0.3 %, $p < 0.001$). Hence, the 10^{-6} M RO-31 is the minimal effective single concentration of RO-31. Furthermore, the inhibition profile of RO-31 demonstrates a steeper decline in S6c contractility compared to Trametinib, as a pronounced reduction occurs between 10^{-6} and 10^{-5} M, suggesting an on/off-like mechanism of action. (Fig. 3d).

Based on the data from the WB and the different kinetics in the S6c inhibition when comparing MEK and PKC inhibition, we hypothesized that RO-31 could potentiate the inhibitory effect of Trametinib. We therefore combined the minimum effective concentrations of RO-31 (10^{-6} M) and Trametinib (10^{-8} M). As can be observed in the sample traces (Fig. 3e), these two inhibitors were additive as the combination of 10^{-6} M RO-31 and 10^{-8} M Trametinib resembled the single effect of 10^{-7} M of Trametinib. We followed up with a concentration response to Trametinib (10^{-10} M – 10^{-6} M) in the presence of 10^{-6} M RO-31 (Fig. 3f). The data show a 10-fold shift in the $logEC_{50}$ for S6c induced

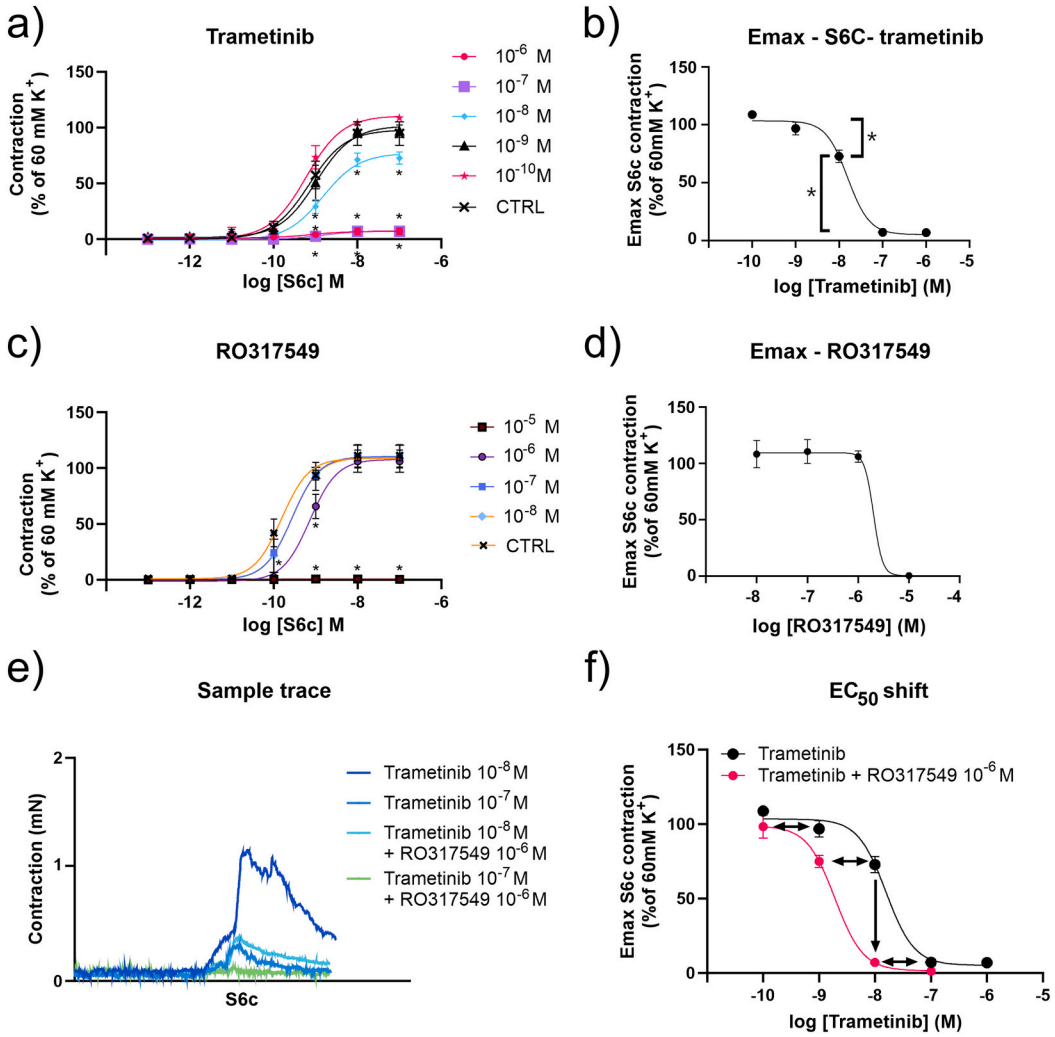

Fig. 3. Comparison of the effects of the MEK inhibitor Trametinib and PKC inhibitor, RO-317549 to the S6C-mediated contraction of BAs after a 48-h OC. (a) Log concentration-response curves in response to S6c, following incubation with 10^{-10}–10^{-6} M Trametinib, (b) $E_{max(S6c)}$ responses of BAs incubated with different concentrations of Trametinib, (c) Log concentration-response curves in response to S6c, following incubation with 10^{-8}–10^{-5} M RO-317549 [16], (d) $E_{max(S6c)}$ responses of BAs incubated with different concentrations of RO-317549, (e) $E_{max(S6c)}$ responses of BAs incubated with different concentrations of Trametinib, and combination of RO-317549 10^{-6} M with different concentrations of Trametinib. The Trametinib curve is the same as shown in panel b. The HillSlope was fixed at −1.727, (f) Representative Sample Traces from LabChart. CTRL refers to BAs incubated for a 48-h in OC with DMSO/Vehicle. Data are shown as mean ± SEM (Biological replicate; n = 5–18). Values were compared with a Student's t-test with a multiple correction (Holm-Sidak). * = $p < 0.05$.

contractility ($E_{max(S6c)}$ values) with single concentrations of Trametinib having a $logEC_{50}$ of −7.8 (95 % CI: −7.93 to −7.63) compared with the combination of 10^{-6} M of RO-31 having a $logEC_{50}$ of −8.72 (95 % CI: −8.85 to −8.53). Combining 10^{-9} M Trametinib with 10^{-6} M RO-31 resulted in an $E_{max(S6c)}$ of 74.9 ± 4.2 %, which is similar ($p = 0.8$) to that of 10^{-8} M of Trametinib ($E_{max(S6c)}$ = 72.8 ± 5.4 %). Moreover, the combination of 10^{-8} M Trametinib with 10^{-6} M RO-31 resulted in an $E_{max(S6c)}$ of 7.1 ± 1.8 %, mimicking the single effect of 10^{-7} M of Trametinib ($E_{max(S6c)}$ = 7.1 ± 2.1 %, $p = 1$). These results support the hypothesis that the PKC inhibitor RO-31 has an additive effect to the MEK inhibition by Trametinib in the OC model, when evaluated by S6c-induced contraction in the myograph.

3.4. *Effect of different ERK inhibitors*

Based on the WB data, the MEK inhibitor Trametinib was able to inhibit the ERK activation/phosphorylation. Since the initial studies were performed in the OC model, newly developed ERK inhibitors have become available. We therefore set out to evaluate the available ERK inhibitors in the OC model. We incubated BAs with Ravoxertinib (GDC-0994), Temuterkib (LY3214996), or Ulixertinib (BVD-523), all at 10^{-6} M, and after 48 h we evaluated the contractility to S6c in the myograph (Fig. 4a).

The BAs incubated in the presence of vehicle showed strong contractility induced by S6c ($E_{max(S6c)}$ = 112.1 ± 5.9 %). The presence of the ERK inhibitor Ravoxertinib in the OC, resulted in an $E_{max(S6c)}$ of 46.8 ± 10 %, significantly different from the vehicle $p < 0.001$, which was similar to the inhibitory effect induced by the presence of the ERK inhibitor Temuterkib ($E_{max(S6c)}$ = 56.2 ± 22 %, $p = 0.49$). However, the BAs incubated with the ERK inhibitor Ulixertinib, resulted in an $E_{max(S6c)}$ of only 13.9 ± 7 %, which was significantly different not only from the control ($p < 0.001$), but also from Ravoxertinib ($p < 0.01$) and Temuterkib ($p = 0.02$). Therefore, we set out to obtain a full concentration response curve for Ulixertinib (10^{-9} M – 10^{-5} M).

As previously observed, S6c induced a contraction in BAs incubated in the presence vehicle ($E_{max(S6c)}$ = 112.1 ± 6 %), (Fig. 4b). The three lowest concentrations did not affect the S6c-induced contraction (10^{-9} M, $E_{max(S6c)}$ = 116.3 ± 6 %, $p = 0.6$), (10^{-8} M, $E_{max(S6c)}$ = 120 ± 5 %, $p = 0.3$), (10^{-7} M, $E_{max(S6c)}$ = 100.4 ± 4 %, $p = 0.2$). The BAs incubated with 10^{-6} M of Ulixertinib resulted in significant reduction of the

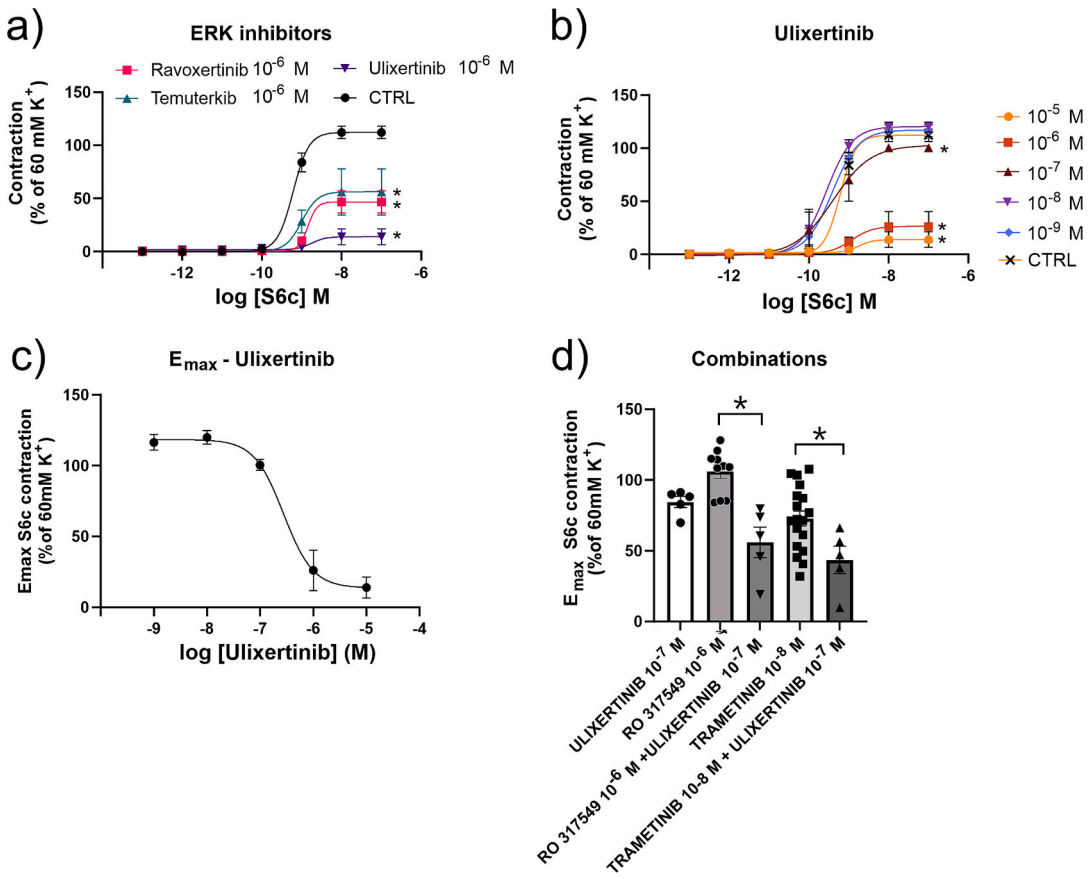

Fig. 4. The effect of different ERK inhibitors on S6c-mediated contraction of BAs incubated in OC for 48 h. (a) Log concentration-response curves in response to S6c, following incubation with the ERK inhibitors Ravoxertinib, (GDC-0994), Temuterkib (LY3214996) and Ulixertinib (BVD-523) at 10^{-6} M, the E_{max} was compared by a multiple *t*-test with a Holm-Sidak correction, (b) Log concentration-response curves in response to S6c, following incubation with 10^{-9}–10^{-5} M Ulixertinib the E_{max} was compared by a multiple t-test with a Holm-Sidak correction (c) $E_{max(S6c)}$ responses to S6c of BAs incubated with different concentrations of Ulixertinib, (d) $E_{max(S6c)}$ responses to S6c of BAs incubated with the combinations of Ulixertinib 10^{-7} M and RO-317549 (10^{-6} M), and Ulixertinib (10^{-7} M) and Trametinib (10^{-8} M). E_{max} compared by one-way ANOVA, with Dunnett's post-test. Data are shown as mean ± SEM (Biological replicate; $n = 4$–18). * = $p < 0.05$.

contractility ($E_{max(S6c)}$ = 26.1 ± 14 %, p < 0.001). The highest concentration 10^{-5} M of Ulixertinib also abolished the contractility effect of S6c ($E_{max(S6c)}$ = 13.9 ± 7 %, p < 0.001), but not significantly different from the 10^{-6} M Ulixertinib ($p = 0.5$). However, the 10^{-5} M concentration affected the overall contractility, with the 60 mM K^+ resulting in mean of 0.08 ± 0.02 mN (p < 0.01 from vehicle, suppl. table1). Of note, the concentration curve for the $E_{max(S6c)}$ values of Ulixertinib with $logEC_{50}$ of −6.520 (95 % CI: −6855 to −6.191) is significant different from the $E_{max(S6c)}$ concentration curve of Trametinib which was −7.8 (95 % CI: −7.93 to −7.63).

To further investigate the possible interplay and feedback between the MEK-ERK1/2 and PKC pathways, we continued with an experiment where we combined the ERK inhibitor, Ulixertinib, with the MEK inhibitor, Trametinib, or the PKC inhibitor, RO-31 (Fig. 4d). The single effect of 10^{-6} M RO-31 ($E_{max(S6c)}$ = 106.1 ± 5 %) was significantly different from the combination of 10^{-6} M RO-31 and 10^{-7} M Ulixertinib ($E_{max(S6c)}$ = 55.9 ± 11 %, $p < 0.0001$). Moreover, the single effect of 10^{-8} M Trametinib ($E_{max(S6c)}$ = 72.8 ± 5 %) was significant different from the combination of the 10^{-8} M Trametinib and the 10^{-7} M Ulixertinib ($E_{max(S6c)}$ = 43.5 ± 10 %, p = 0.02). The combination of the 10^{-6} M RO-31 and 10^{-7} M Ulixertinib was not significant different from the combination of 10^{-8} M Trametinib and the 10^{-7} M Ulixertinib (p = 0.42). These results showed that the ERK inhibitor is additive for both the PKC and MEK pathways.

3.5. Effect of the NF-κB inhibitor BMS 345541

We showed above that adding a downstream inhibitor of the MEK pathway was additive, and further WB data suggested that RO-31 was linked to activation of NF-κB. We incubated BAs with different NF-κB inhibitors, IMD 0354, SP100030 and BMS 345541, all at 10^{-6} M, and the evaluation of the contractility was done after 48 h, with S6c in the myograph, and compared to vehicle (Fig. 5a).

The BAs incubated with vehicle resulted in $E_{max(S6c)}$ of 100.5 ± 7 %. IMD 0354 has previously been studied in the literature, and even though the 10^{-6} M concentration had an inhibitory effect ($E_{max(S6c)}$ = 66.7 ± 9 %, $p = 0.06$), it greatly reduced the overall contractility (60 mM K^+ mN, supplementary table 1) therefore, this inhibitor was not pursued further. The presence of the SP100030 (10^{-6} M), a dual inhibitor of AP-1 and NF-κB, in the OC resulted in an $E_{max(S6c)}$ of 106.5 ± 3 %, which was not significantly different from the vehicle ($p = 0.7$). For the BAs incubated with the BMS 345541, an IkB/IKK specific inhibitor, we also did not observe an effect at 10^{-6} M ($E_{max(S6c)}$ = 93 ± 10 %, $p = 0.6$). Nevertheless, we decided to test a higher concentration BMS 345541 (10^{-5} M), and at this concentration the contraction to S6c was abolished ($E_{max(S6c)}$ = 3.3 ± 3 %, $p < 0.001$, Fig. 5b).

To investigate possible interplay, we combined the 10^{-6} M RO-31 and/or the 10^{-8} M Trametinib, with the 10^{-6} M BMS 345541. It was observed that the single effect of the 10^{-6} M RO-31 ($E_{max(S6c)}$ = 106.1 ± 5 %) was significantly different ($p = 0.02$) from the combination of the 10^{-6} M RO-31 with the 10^{-6} M BMS 345541 ($E_{max(S6c)}$ = 68.7 ± 9 %). Further, the single effect of 10^{-8} M Trametinib ($E_{max(S6c)}$ = 72.8 ± 5 %),

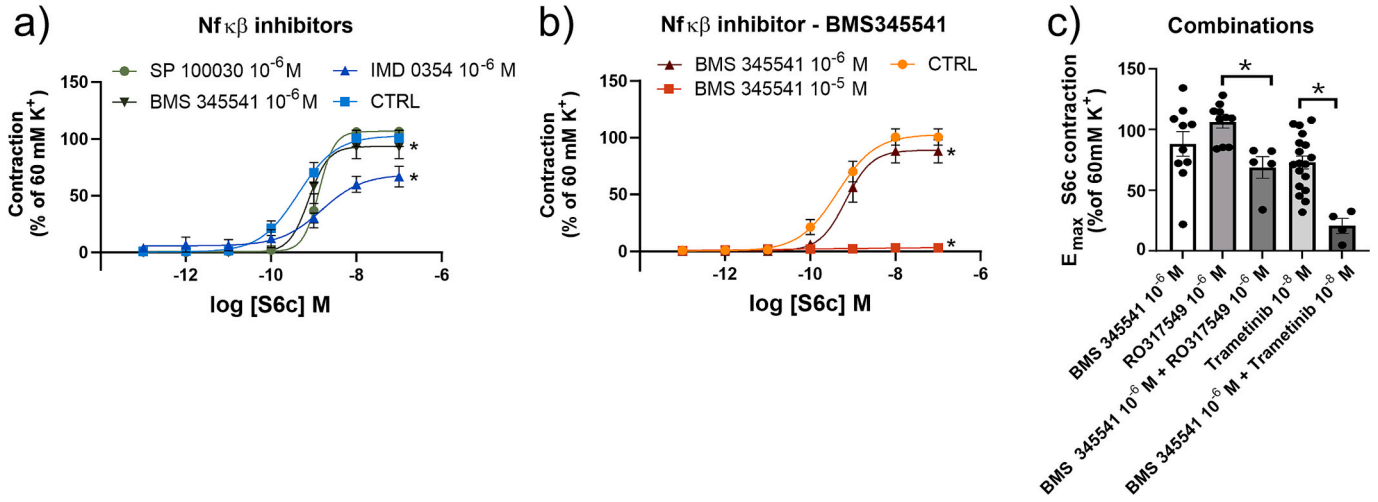

Fig. 5. The effect of NF-κB inhibitors in the contractility of BAs incubated for 48 h in OC. (a) Log concentration-response curves in response S6c, following incubation with the NF-κB inhibitors SP100030, BMS 345541, IMD 0354 (10^{-6} M) the E_{max} was compared by a multiple *t*-test with a Holm-Sidak correction (b) Log-concentration-response curves in response to S6c following incubation with 10^{-5} M and 10^{-6} M BMS 345541, the E_{max} was compared by a multiple t-test with a Holm-Sidak correction (c) $E_{max(S6c)}$ contractions of RO317549 10^{-6} M, BMS 345541 10^{-6} M and their combination, compared with Trametinib 10^{-8} M and its combination with BMS 345541 10^{-6} M. E_{max} were compared by one-way ANOVA, with Dunnett's post-test. Data are shown as mean ± SEM (Biological replicate; n = 4–18). * = $p < 0.05$.

was also significant different ($p = 0.002$) from the combination of the 10^{-8} M Trametinib with the 10^{-6} M BMS 345541 ($E_{max(S6c)} = 20.8 \pm 6$ %), likewise to what we observed for the ERK inhibitor. After comparing the two combinations, we observed that the difference between them was 47.97 ± 12 %, ($p = 0.004$), indicating that the additive effect of Trametinib is significantly more potent than that of RO-31.

3.6. Effect of time

It is known that time is an important factor for the activation of the signaling pathways. To investigate the order of activation in the above pathways, the inhibitors we used in the previous experiments, were added either at time 0 or delayed, after the arteries had been incubated in OC with DMEM for 6 h (Fig. 6a). The 6-h time point was selected both based on the western blot data, and to reflect the clinical situation in embolic stroke, where currently approved treatments, such as thrombolysis or thrombectomy, are not administered beyond this window [26,27]. As no effective therapies are available after 6 h, identification of molecular targets that remain responsive at this later stage may be of therapeutic relevance [1].

S6c induced a contraction in the BAs incubated both when the vehicle had been added at time 0 ($E_{max(S6c)} = 94.7 \pm 11$ %) or delayed 6 h ($E_{max(S6c)} = 77 \pm 12$ %, $p = 0.4$). 10^{-7} M Trametinib at time 0 had a significant effect compared to time 0 vehicle ($E_{max(S6c)} = 7.1 \pm 2$ %, $p = 0.003$). When 10^{-7} M trametinib was added at 6 h, its inhibitory actions were significantly ($p = 0.003$) reduced ($E_{max(S6c)} = 51.3 \pm 9$ %). Moreover, this inhibitory effect was not significantly different from the 6 h vehicle ($p = 0.1$) indicating that the MEK inhibitor is not effective if added at the delayed time point of 6 h. The data from the time 0 is from the previous experiments.

10^{-5} M RO-31 at time 0 abolished the S6c-mediated contractile effect compared to the vehicle at time 0 ($E_{max(S6c)} = 0.46 \pm 0.3$ %, $p < 0.001$).

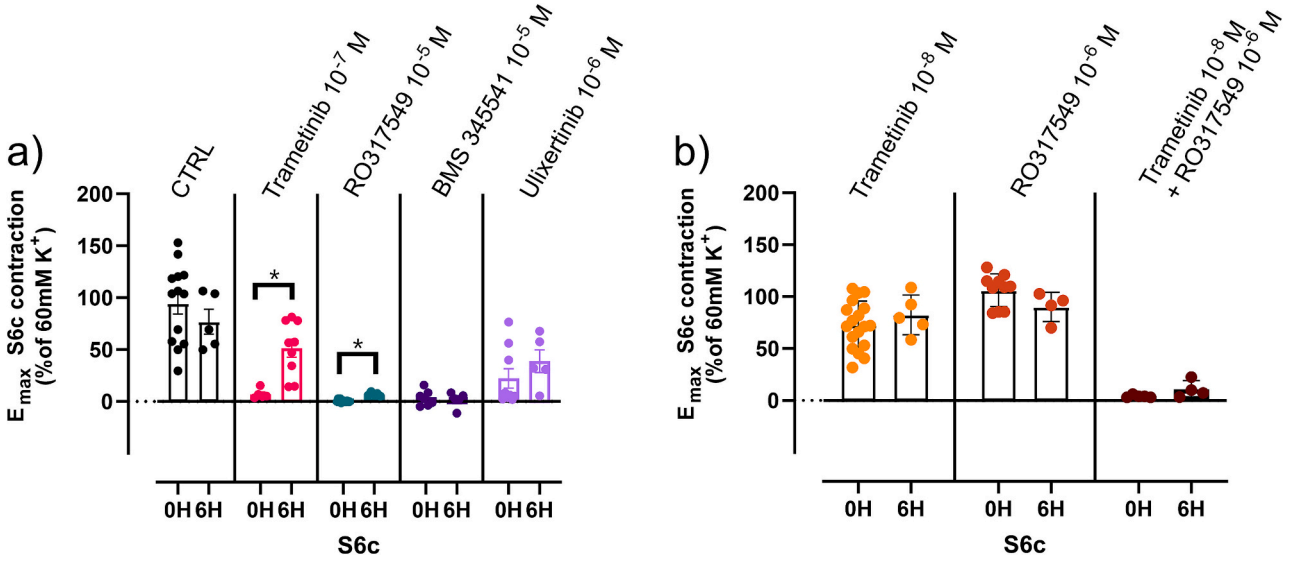

Fig. 6. Time-dependent effects of inhibitor addition (a) Addition of the different inhibitors at different time points 0 h or delayed 6 h. (b) Combination of 10^{-8} M Trametinib and 10^{-6} M RO-31 at time 0 or delayed 6 h, the control experiment is in panel a. Data are shown as mean ± SEM (Biological replicate; n = 4–18). The E_{max} were compared by Student's *t*-test. * = $p < 0.05$.

When added at 6 h, the 10^{-5} M RO-31 resulted in $E_{max(S6c)}$ of 7 ± 0.8 %, which was significant different from the time 0 ($p < 0.001$), even though it was still effective compared to 6 h vehicle ($p < 0.001$). These data showed that the PKC inhibition is not very time sensitive in the 0 to 6-h window.

Furthermore, 10^{-5} M BMS 345541 at time 0 resulted in inhibition of the S6c-mediated contractile effect ($E_{max(S6c)} = -0.2 \pm 2$ %, $p < 0.001$). The 6 h delayed time did not affect the inhibitory ability of the 10^{-5} M BMS 345541 ($E_{max(S6c)} = 4.8 \pm 3$ %, $p = 0.3$) compared to time 0, indicating that the effectiveness is not time dependent, similarly as for PKC inhibition.

The S6c-mediated contractility was also inhibited by 10^{-6} M Ulixertinib at time 0 ($E_{max(S6c)} = 22.9 \pm 9$ %, $p < 0.001$) compared to vehicle, and as well as at the delayed 6-h time point ($E_{max(S6c)} = 38.7 \pm 11$ %,) with no significant difference from the time 0 ($p = 0.3$).

We next set out to investigate whether the combinations of the single lowest effective dose of Trametinib and RO-31 could have a potential inhibitory effect when added at 6 h (Fig. 6b). 10^{-8} M Trametinib at time 0 resulted in $E_{max(S6c)}$ of 71.4 ± 6 % which was significant different from the vehicle ($p = 0.047$). Added at 6 h, an $E_{max(S6c)}$ of 82.4 ± 9 % was the result of 10^{-8} M Trametinib, which was not significant different ($p = 0.3$) from time 0 or from the vehicle at 6 h ($p = 0.7$), indicating that the single effect of 10^{-8} M Trametinib was not effective at 6 h. At time 0, 10^{-6} M RO-31 resulted in an $E_{max(S6c)}$ of 106.1 ± 5 % which is not significant different from the vehicle ($p = 0.4$). As a side note here, the previous significant change at this dose was observed at 10^{-10} and 10^{-9} M S6c making it the minimum single effective concentration of RO-31. At 6 h, there was still no effect of a single dose of 10^{-6} M RO-31 result compared to time 0 ($E_{max(S6c)} = 90 \pm 7$ %, $p = 0.1$). Similar as before, the combination of 10^{-8} M Trametinib and 10^{-6} M RO-31 at time 0, resulted in $E_{max(S6c)}$ of 4.1 ± 0.6 % which was significantly different from the vehicle ($p < 0.001$). The same combination, when added at 6 h, strongly inhibited the S6c-mediated contraction ($E_{max(S6c)} = 10.8 \pm 4$ %) not different from that at time 0 ($p = 0.1$). Interestingly, the loss of inhibition observed with trametinib at 6 h, can be compensated by adding a PKC inhibitor, as the inhibition of the S6c-mediated contraction, compared to vehicle was robust ($p = 0.002$), suggesting a potential feedback activation by PKC.

4. Discussion

In this study, the pathways behind the upregulation of the ET_B receptor following flow cessation, were investigated in detail using a broad pharmacological approach. MEK and PKC were shown to represent two distinct pathways, activated sequentially, challenging the prevailing view on their interplay. These findings could have implications for understanding vascular pathology.

The study demonstrated that the MEK-ERK1/2 signaling pathway and the PKC pathway play key roles in regulating ET_B receptor upregulation during flow cessation. PKC activation is assumed to precede MEK activation [28,29], however, this relationship has not been explored in vascular smooth muscle cells in OC. Western blot analysis showed that inhibiting PKC did not reduce ERK phosphorylation but did reduce NF-κB phosphorylation, suggesting parallel pathway activation. Conversely, MEK inhibitors effectively reduced ERK phosphorylation without affecting NF-κB phosphorylation, emphasizing the distinct roles of these pathways in regulating ET_B receptor function (Fig. 2).

Given evidence of parallel MEK and PKC pathways, their combined roles in ET_B receptor upregulation were further explored. Trametinib, a potent MEK inhibitor [18], reduced receptor upregulation more effectively than RO-31, a PKC inhibitor. Combining a minimal effective concentration of RO-31 with Trametinib shifted the concentration curve tenfold (Fig. 3f), indicating additive effects of MEK and PKC inhibition. Novel ERK inhibitors such as Ravoxertinib, Temuterkib, and Ulixertinib [30–33] reduced ET_B receptor upregulation but showed lower potency in OC compared to cell-free assays (Fig. 4) [34,35]. These discrepancies may result from metabolism or nuclear mechanisms. Concurrent inhibition of MEK, ERK, and PKC demonstrated synergistic effects, aligning with findings of negative feedback in the MEK-ERK1/2 pathway [36–38].

The role of NF-κB inhibitors, downstream components of the PKC pathway, was investigated using BMS345541, SP100030, and IMD0354, selected based on previous studies [15,39–41]. BMS345541 and SP100030 showed limited effects, while IMD0354 significantly reduced contractility. As NF-κB functions downstream of PKC, combining BMS345541 with MEK inhibitors mirrored the effects of combining PKC inhibitors with MEK inhibitors, consistent with their position within the pathway (Fig. 5). These findings reinforce the concept that MEK and PKC are separate pathways. The time-dependent dynamics of pathway activation were also examined. Delayed introduction of MEK inhibitors (6 h post-isolation) reduced efficacy compared to immediate addition, while PKC inhibitors remained effective when introduced later (Fig. 6). These findings suggest that MEK acts earlier in the cascade, while PKC serves as a delayed regulator of transcription.

The present results support the conclusion that MEK and PKC signaling function independently rather than sequentially in vascular smooth muscle under ischemia-like conditions. Selective inhibition of PKC isoforms (PKC-α, βI, βII, γ, ε) with RO-317549 did not alter ERK phosphorylation, demonstrating that MEK–ERK activation occurs independently of these PKC isoforms (Figs. 2 and 3). Other broader inhibitors of PKC, such as Go6983 (inhibitor of PKCα, PKCβ, PKCγ and PKCδ) has been shown to inhibit MEK activation in other systems [42], suggesting that this could be subtype specific. A limitation of the present study is that only one PKC inhibitor, RO-317549, was used to investigate the role of PKC signaling. Although the findings support independent activation of PKC and MEK pathways, confirmation using an additional PKC inhibitor from a different structural class, such as a c1-, c2-, or c3-domain binding inhibitor, would strengthen the conclusions. Investigation of additional inhibitors should be considered in future studies to further validate the observed pathway separation.

MEK inhibition with Trametinib reduced ERK phosphorylation but did not affect PKC-dependent NF-κB activation, reinforcing pathway separation (Fig. 2). This independence contrasts with earlier findings in non-vascular cells, where PKC typically activates MEK through Raf phosphorylation [28,29,43]. Additionally, additive effects from combined PKC and MEK inhibition in our study provided further evidence against sequential signaling. It is important to note that in other studies, synergistic effects to MEK have often been attributed to separate pathways [44,45]. Differences in time-based sensitivity to inhibitors, with PKC inhibition remaining effective at later time points than MEK inhibition, further support the notion of independent and temporally distinct activation (Fig. 6). In lymphocytes, there is evidence that there are two distinct pathways activating ERK, one for the acute and one for the long-term activation, or it could be the case of sequential binding of transcription factors [46].

These findings support a model in which flow cessation initiates two temporally and mechanistically distinct signaling pathways that converge on ET_B receptor upregulation in vascular smooth muscle (Fig. 7). The MEK–ERK1/2 cascade is activated early, likely via RAS–RAF signaling, and is sensitive to inhibition by Trametinib or Ulixertinib. In contrast, a delayed rise in intracellular Ca^{2+} promotes PKC activation, which in turn facilitates NF-κB signaling through the IKK complex. Notably, PKC and NF-κB inhibition remain effective even when applied several hours after the initial stimulus, indicating that this pathway is temporally delayed. The additive effects observed with combined inhibition of both pathways argue against a strictly sequential relationship and instead suggest functional independence with convergence at the level of transcriptional regulation. This parallel activation enhances the robustness of the response and underscores the requirement for both pathways to achieve full ET_B receptor induction and downstream functional effects. These results expand the understanding of a part of ischemia-induced signaling, induced by flow cessation, by

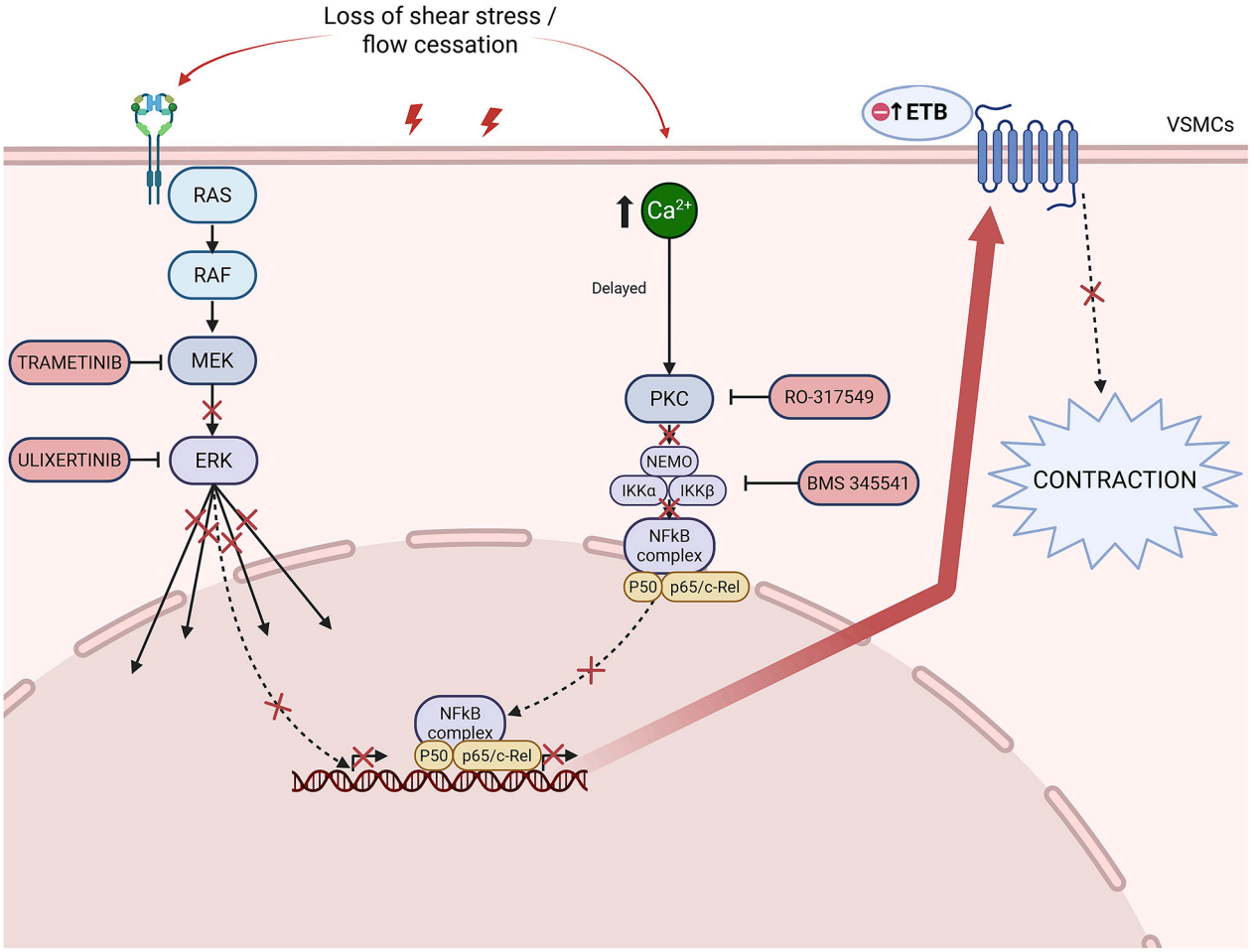

Fig. 7. Signaling pathways involved in ET_B receptor upregulation and VSMC contraction. Extracellular stimuli such as flow cessation activate the MAPK/ERK pathway, which is disrupted by MEK inhibition (Trametinib) or ERK inhibition (Ulixertinib). In parallel, intracellular Ca^{2+} increase leads to delayed PKC activation, promoting NF-κB signaling via the IKK complex. PKC and NF-κB inhibition (RO-317549 and BMS345541, respectively) remain effective when applied up to 6 h post-stimulus. Combined inhibition further suppresses ET_B upregulation on VSMCs and reduces receptor-mediated contraction, indicating that both pathways contribute independently and are required for full functional response. Abbreviations: ET_B: endothelin type B receptor; VSMC: vascular smooth muscle cell; NF-κB: nuclear factor. Created in BioRender. Kazantzi, S. (2025) https://BioRender.com/u89c445

illustrating how early and delayed signaling modules are integrated to control vascular reactivity.

This study challenges the dominant view that PKC is the primary activator of MEK in VSMCs. It showed that a PKC inhibitor does not inhibit MEK phosphorylation but effectively prevent ET_B receptor upregulation, even when added 6 h after flow cessation. MEK inhibitors were less effective at this delayed time point, reinforcing the idea that PKC functions as a delayed regulator. The additive effects observed with combined pathway inhibition underscore their therapeutic potential for addressing ET_B receptor-mediated vascular pathologies associated with ischemia caused by flow cessation. To expand on the clinical implications, decades of research have underscored the potential of targeting pathways involved in ET_B receptor upregulation and vascular responses to flow cessation. MEK and PKC inhibitors have shown efficacy in rodent models, and similar mechanisms occur in human cerebral arteries [47,48]. Clinical trials, including those investigating MEK1/2 inhibitors for aSAH patients (EudraCT 2013–003690-10), further validate these findings. For example, the STOP-DCI trial uses U0126, a MEK1/2 inhibitor, administered at multiple time points post-SAH [49,50].

5. Conclusion

In conclusion, this study redefines the regulation of ET_B receptor upregulation in vascular pathologies, demonstrating that MEK and PKC function as parallel and distinct pathways rather than in sequence. PKC does not influence MEK phosphorylation, but instead acts as a delayed regulator, while MEK operates earlier in the signaling cascade. These findings demonstrate that MEK-ERK1/2 and PKC pathways act independently and contribute additively to ET_B receptor upregulation under conditions of flow cessation. The study provides a mechanistic framework for understanding their distinct roles and temporal characteristics. The effectiveness of delayed PKC inhibition indicates potential relevance for therapeutic intervention for ischemia beyond the acute phase. These results form a basis for future in vivo studies addressing pathway-specific targeting in cerebrovascular disease.

CRediT authorship contribution statement

Spyridoula Kazantzi: Writing – original draft, Visualization, Methodology, Investigation, Formal analysis, Data curation, Conceptualization. **Lars Edvinsson:** Writing – review & editing, Resources, Conceptualization. **Kristian Agmund Haanes:** Writing – review & editing, Visualization, Supervision, Resources, Project administration, Methodology, Formal analysis, Conceptualization.

Declaration of Generative AI and AI-assisted technologies in the writing process

During the preparation of this work, the authors used ChatGPT to improve readability and language. After using this tool/service, the authors reviewed and edited the content as needed and take full responsibility for the content of the publication.

Funding information

This work was supported by the Translational Research Centre, Copenhagen University Hospital – Rigshospitalet, Glostrup, Denmark. Kristian A. Haanes was supported by a Lundbeck Foundation Fellowship (R345–2020-1977).

Declaration of competing interest

The authors declare the following financial interests/personal relationships which may be considered as potential competing interests: Kristian Agmund Haanes reports financial support was provided by Lundbeck Foundation. Lars Edvinsson reports a relationship with Edvince AB, Sweden that includes: board membership and equity or stocks. Lars Edvinsson has patent #MEK INHIBITOR FOR TREATMENT OF STROKE - 20220273660 pending to Lars EDVINSSON. Lars Edvinsson has patent #Ischemic disorder or disease inhibitors -8273771 issued to Pronas Pharma AB. Lars Edvinsson has patent #ISCHEMIC DISORDER OR DISEASE INHIBITORS - 20100152248 pending to Pronas Pharma AB. All authors declare no conflicts of interest pertaining to the submitted work. If there are other authors, they declare that they have no known competing financial interests or personal relationships that could have appeared to influence the work reported in this paper.

Appendix A. Supplementary data

Supplementary data to this article can be found online at https://doi.org/10.1016/j.jmccpl.2025.100300.

References

[1] Maddahi A, Edvinsson L. Enhanced expressions of microvascular smooth muscle receptors after focal cerebral ischemia occur via the MAPK MEK/ERK pathway. BMC Neurosci 2008;9(1):85.
[2] Edvinsson L. Cerebrovascular endothelin receptor upregulation in cerebral ischemia. Curr Vasc Pharmacol 2009;7(1):26–33.
[3] Edvinsson LI, Povlsen GK. Vascular plasticity in cerebrovascular disorders. J Cereb Blood Flow Metab 2011;31(7):1554–71.
[4] Macdonald RL. Delayed neurological deterioration after subarachnoid haemorrhage. Nat Rev Neurol 2014;10(1):44–58.
[5] Liu, S., et al., *Endothelin-1 Activates Endothelial Cell Nitric-oxide Synthase via Heterotrimeric G-protein βγ Subunit Signaling to Protein Kinase B/Akt* *. J Biol Chem, 2003. 278(50): p. 49929–49935.
[6] Nilsson D, et al. Endothelin receptor-mediated vasodilatation: effects of organ culture. Eur J Pharmacol 2008;579(1–3):233–40.
[7] Bautista-Niño PK, et al. Local endothelial DNA repair deficiency causes aging-resembling endothelial-specific dysfunction. Clin Sci (Lond) 2020;134(7):727–46.
[8] Skovsted GF, et al. Heart ischaemia-reperfusion induces local up-regulation of vasoconstrictor endothelin ETB receptors in rat coronary arteries downstream of occlusion. Br J Pharmacol 2014;171(11):2726–38.
[9] Skovsted GF, et al. Rapid functional upregulation of vasocontractile endothelin ETB receptors in rat coronary arteries. Life Sci 2012;91(13–14):593–9.
[10] Povlsen GK, et al. In vivo experimental stroke and in vitro organ culture induce similar changes in vasoconstrictor receptors and intracellular calcium handling in rat cerebral arteries. Exp Brain Res 2012;219(4):507–20.
[11] Stenman E, et al. Cerebral ischemia upregulates vascular endothelin ET(B) receptors in rat. Stroke 2002;33(9):2311–6.
[12] Nilsson D, et al. Up-regulation of endothelin type B receptors in the human internal mammary artery in culture is dependent on protein kinase C and mitogen-activated kinase signaling pathways. BMC Cardiovasc Disord 2008;8:21.
[13] Henriksson M, Stenman E, Edvinsson L. Intracellular Pathways Involved in Upregulation of Vascular Endothelin Type B Receptors in Cerebral Arteries of the Rat. Stroke 2003;34(6):1479–83.
[14] Henriksson M, Xu C-B, Edvinsson L. Importance of ERK1/2 in upregulation of endothelin type B receptors in cerebral arteries. Br J Pharmacol 2004;142(7):1155–61.
[15] Sandhu H, Ansar S, Edvinsson L. Comparison of MEK/ERK pathway inhibitors on the upregulation of vascular G-protein coupled receptors in rat cerebral arteries. Eur J Pharmacol 2010;644(1):128–37.
[16] Bömers JP, et al. Protein kinase C-inhibition reduces critical weight loss and improves functional outcome after experimental subarachnoid haemorrhage. J Stroke Cerebrovasc Dis 2024;33(7):107728.
[17] Bömers JP, et al. The MEK Inhibitor Trametinib Improves Outcomes following Subarachnoid Haemorrhage in Female Rats. Pharmaceuticals 2022;15(12):1446.
[18] Christensen ST, et al. Pre-clinical effects of highly potent MEK1/2 inhibitors on rat cerebral vasculature after organ culture and subarachnoid haemorrhage. Clin Sci 2019;133(16):1797–811.
[19] Yamaguchi T, et al. Antitumor activities of JTP-74057 (GSK1120212), a novel MEK1/2 inhibitor, on colorectal cancer cell lines in vitro and in vivo. Int J Oncol 2011;39(1):23–31.
[20] Ward RA, et al. Structure-Guided Design of Highly Selective and Potent Covalent Inhibitors of ERK1/2. J Med Chem 2015;58(11):4790–801.
[21] Wilkinson, S.E., P.J. Parker, and J.S. Nixon, Isoenzyme specificity of bisindolylmaleimides, selective inhibitors of protein kinase C. Biochem J, 1993. 294 (**Pt 2)**(Pt 2): p. 335–7.
[22] Burke JR, et al. BMS-345541 is a highly selective inhibitor of I kappa B kinase that binds at an allosteric site of the enzyme and blocks NF-kappa B-dependent transcription in mice. J Biol Chem 2003;278(3):1450–6.
[23] Högestätt ED, Andersson KE, Edvinsson L. Mechanical properties of rat cerebral arteries as studied by a sensitive device for recording of mechanical activity in isolated small blood vessels. Acta Physiol Scand 1983;117(1):49–61.
[24] Zheng JP, et al. NF-kappaB signaling mediates vascular smooth muscle endothelin type B receptor expression in resistance arteries. Eur J Pharmacol 2010;637(1–3):148–54.
[25] Zhang W, et al. Transcriptional down-regulation of thromboxane A(2) receptor expression via activation of MAPK ERK1/2, p38/NF-kappaB pathways. J Vasc Res 2009;46(2):162–74.
[26] Powers WJ, et al. 2015 American Heart Association/American Stroke Association Focused Update of the 2013 Guidelines for the Early Management of Patients With Acute Ischemic Stroke Regarding Endovascular Treatment: A Guideline for Healthcare Professionals From the American Heart Association/American Stroke Association. Stroke 2015;46(10):3020–35.
[27] Rehani B, et al. A New Era of Extended Time Window Acute Stroke Interventions Guided by Imaging. Neurohospitalist 2020;10(1):29–37.
[28] Scerri J, et al. PKC-mediated phosphorylation and activation of the MEK/ERK pathway as a mechanism of acquired trastuzumab resistance in HER2-positive breast cancer. Front Endocrinol (Lausanne) 2022;13:1010092.
[29] Ueda Y, et al. Protein kinase C activates the MEK-ERK pathway in a manner independent of Ras and dependent on Raf. J Biol Chem 1996;271(38):23512–9.
[30] Sullivan RJ, et al. First-in-Class ERK1/2 Inhibitor Ulixertinib (BVD-523) in Patients with MAPK Mutant Advanced Solid Tumors: Results of a Phase I Dose-Escalation and Expansion Study. Cancer Discov 2018;8(2):184–95.
[31] Song Y, et al. ERK inhibitor: A candidate enhancing therapeutic effects of conventional chemo-radiotherapy in esophageal squamous cell carcinoma. Cancer Lett 2023;554:216012.
[32] Grogan L, Shapiro P. Chapter Five - Progress in the development of ERK1/2 inhibitors for treating cancer and other diseases. In: Slusher BS, Peters DE, editors. Advances in Pharmacology. Academic Press; 2024. p. 181–207.
[33] Timofeev O, et al. ERK pathway agonism for cancer therapy: evidence, insights, and a target discovery framework. npj Precision. Oncology 2024;8(1):70.
[34] Lebraud H, et al. Quantitation of ERK1/2 inhibitor cellular target occupancies with a reversible slow off-rate probe. Chem Sci 2018;9(45):8608–18.
[35] Huang Y, et al. Vascular endothelial growth factor enhances tendon-bone healing by activating Yes-associated protein for angiogenesis induction and rotator cuff reconstruction in rats. J Cell Biochem 2020;121(3):2343–53.
[36] Sagoo MS, et al. Combined PKC and MEK inhibition for treating metastatic uveal melanoma. Oncogene 2014;33(39):4722–3.
[37] Barbosa R, Acevedo LA, Marmorstein R. The MEK/ERK Network as a Therapeutic Target in Human Cancer. Mol Cancer Res 2021;19(3):361–74.
[38] Song Y, et al. Targeting RAS–RAF–MEK–ERK signaling pathway in human cancer: Current status in clinical trials. Genes & Diseases 2023;10(1):76–88.
[39] Sandhu H, Xu CB, Edvinsson L. Upregulation of contractile endothelin type B receptors by lipid-soluble cigarette smoking particles in rat cerebral arteries via activation of MAPK. Toxicol Appl Pharmacol 2010;249(1):25–32.
[40] Lei Y, et al. Up-regulation of bradykinin receptors in rat bronchia via IκB kinase-mediated inflammatory signaling pathway. Eur J Pharmacol 2010;634(1):149–61.
[41] Ye N, et al. Small molecule inhibitors targeting activator protein 1 (AP-1). J Med Chem 2014;57(16):6930–48.
[42] Tian T, et al. Endothelial alpha(1)-adrenergic receptor activation improves cardiac function in septic mice via PKC-ERK/p38MAPK signaling pathway. Int Immunopharmacol 2024;141:112937.
[43] Kolch W, et al. Protein kinase C alpha activates RAF-1 by direct phosphorylation. Nature 1993;364(6434):249–52.
[44] Temblador A, et al. Synergistic targeting of the PI3K/mTOR and MAPK/ERK pathways in Merkel cell carcinoma. Tumour Virus Res 2022;14:200244.
[45] Hoeflich KP, et al. In vivo antitumor activity of MEK and phosphatidylinositol 3-kinase inhibitors in basal-like breast cancer models. Clin Cancer Res 2009;15(14):4649–64.
[46] Ishihara S, Schwartz RH. Two-step binding of transcription factors causes sequential chromatin structural changes at the activated IL-2 promoter. J Immunol 2011;187(6):3292–9.

[47] Ahnstedt H, et al. Human cerebrovascular contractile receptors are upregulated via a B-Raf/MEK/ERK-sensitive signaling pathway. BMC Neurosci 2011;12(1):5.
[48] Ansar S, et al. MAPK signaling pathway regulates cerebrovascular receptor expression in human cerebral arteries. BMC Neurosci 2013;14(1):12.
[49] Christensen ST, et al. Synergistic effects of a cremophor EL drug delivery system and its U0126 cargo in an ex vivo model. Drug Delivery 2019;26(1):680–8.
[50] Edvinsson L, Krause DN. Switching Off Vascular MAPK Signaling: A Novel Strategy to Prevent Delayed Cerebral Ischemia Following Subarachnoid Hemorrhage. Transl Stroke Res 2024.